Supporting Information For

An Open-Source Automated Parahydrogen Hyperpolarizer for Molecular Imaging Using ^{13}C Metabolic Contrast Agents

Aaron M. Coffey,[a] Roman V. Shchepin,[a,b] Milton L. Truong,[a,b] Ken Wilkens,[a] Wellington Pham[a,b,c,d] and Eduard Y. Chekmenev[a,b,c,d,e,*]

[a]Vanderbilt University Institute of Imaging Science (VUIIS), [b]Department of Radiology, [c]Department of Biomedical Engineering, [d]Vanderbilt-Ingram Cancer Center (VICC), Vanderbilt University, Nashville, Tennessee 37232-2310, United States

[e]Russian Academy of Sciences, Leninskiy Prospekt 14, Moscow, 119991, Russia

Corresponding Author

*Eduard Y. Chekmenev,
1161 21st Ave South, MCN-AA1105
Vanderbilt University Institute of Imaging Science
Nashville, TN 37232, USA
Phone: 615-322-1329
Fax: 615-322-0734
E-mail: eduard.chekmenev@vanderbilt.edu

Table of Contents

1. PHIP Hyperpolarizer System Diagram

It was observed that solenoid valve (E, Figure S1) magnetic fields must have the same polarity as the electromagnet (and any post-production magnetized transfer pathway such as a HyperBridge[1]) to mitigate losses of produced hyperpolarization. Use of some AC solenoid valves in proximity to hyperpolarized material results in depolarization.

A controller unit orchestrates sequencing of operations of the manifold with RF spin order transfer sequences. An additional HyperGate[1] constructed underneath the main B_0 magnet of the PHIP polarizer from an array of permanent magnets (K & J Magnetics part BY-Y02, a 2 in. by 2 in. by 1/8 in. NdFeB type magnet) consisted of four magnets at the corners of a 6 in. × 6 in. square of 1/2 in. thick plastic, centered underneath the solenoid electromagnet in the compartment below. These magnets increased the otherwise weak magnetic field covering that portion of the transfer pathway between the electromagnet and the HyperBridge,[2] and are critical to preserving transferred ^{13}C-phospholactate hyperpolarization.

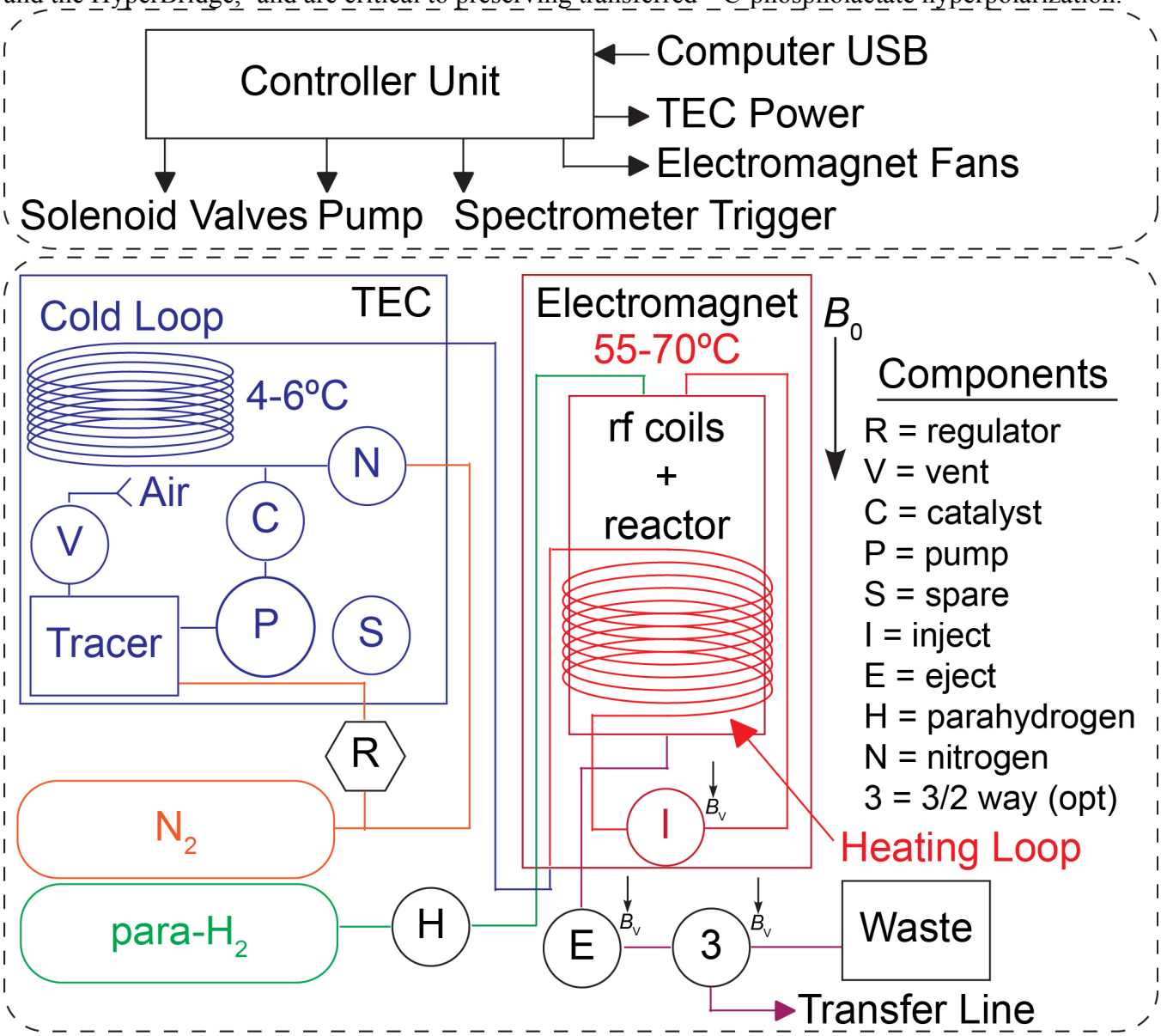

Figure S1. PHIP hyperpolarizer system diagram. The gas/liquid manifold connections, solenoid valves, dispensing pump, and other components such as the controller unit forming the overall system for the PHIP hyperpolarizer are shown. The directionality of the magnetic fields produced by key DC solenoid valves is indicated.

2. PHIP Hyperpolarizer Solenoid Electromagnet for Operation at 5.75 mT

A simple solenoid electromagnet generates the B_0 magnetic field with 5.75 mT strength. The 20 in. long solenoid is wound as a single layer on a G12 fiberglass tube (P/N G12-4I-VL, Rocketry Warehouse, Hollsopple, PA) with 4.025 in. outer diameter and 24 in. length, and consists of 574 turns of 20 AWG magnet wire (P/N 40480, 20-HAPT-200, MWS Wire Industries, Westlake Village, CA). Inside the tube a shield of two layers of 0.008 in. copper (P/N 9709K18, McMaster-Carr) reduces RF interference. The two magnet wire leads are connected to a Schaffner power line filter (P/N 817-1204-ND, Digi-Key Electronics, Thief River Falls, MN) to mitigate line noise passing through the linear power supply and coupling from the magnet into the PHIP probe RF coils. The magnet is powered by a linear power supply model GW Instek GPR-6060D (P/N B005G038YY, Amazon.com).

The solenoid magnet was modeled in MATLAB (Mathworks, Natick, MA) to allow designing the magnet, Figure S2. Design variables included assessing the B_0 field homogeneity and staying within the power supply voltage and current limits. The magnet model consisted of approximating the 574 turn solenoid as a collection of circular wire loops with zero conductor thickness (i.e. ideal current filaments) with spacing $s = L/(n\text{-}1)$, where L is the magnet length and n is the number of turns. The B_0 field was calculated by superposition of the field generated by each loop over space according to the BiotSavart formula for a circular loop.[3] The spatial extent over which the field remained within a specified homogeneity was then determined by calculating ΔB_0 relative to the maximum B_0 at the center of the magnet. A relatively short 20 in. solenoid with a length/diameter ratio of ~5 was deemed sufficient, yielding a theoretical 300 ppm over 3.6 cm and a magnetic field constant of 1.3863 mT/A and a magnet voltage drop of ~6.76 V/A at room temperature for the selected magnetic geometry and magnet wire (Figure S2). Experimental data confirmed the simulations.

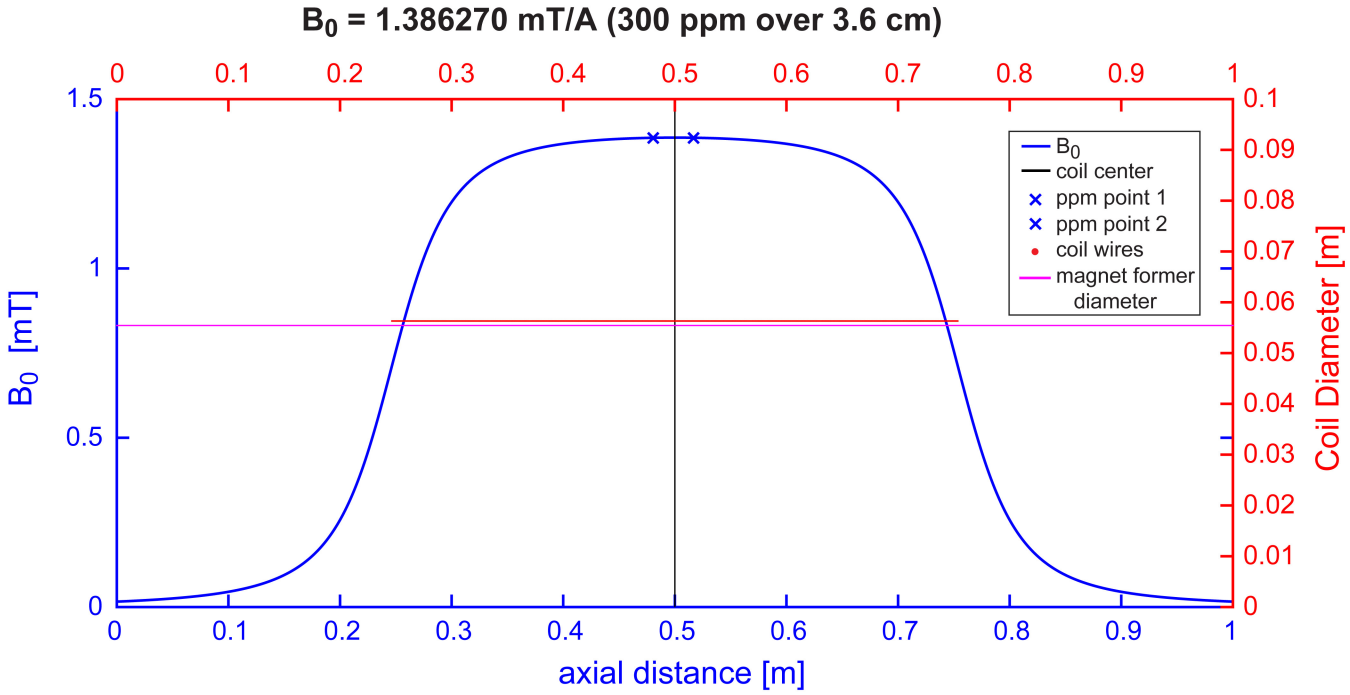

Figure S2. Solenoid electromagnet simulation. The B_0 field per ampere current and its homogeneity (calculated from peak B_0 at magnet center) for the electromagnet were calculated in MATLAB using BiotSavart's law with the solenoid approximated as a collection of ideal circular wire loops spaced 20 AWG wire diameter between centers.

3. PHIP Hyperpolarizer RF Probe Design and Calibration

The ^{1}H excitation and ^{13}C detection RF coils consist of two Helmholtz saddle coils geometrically orthogonal for isolation (~ 15 dB). These coils were not optimized, and were both wound with 16/38 Litz wire (SKU 16/38-Litz, Mike's Electronic Parts, Fairfield, OH). The ^{1}H excitation coil was wound on the inner surface of the polycarbonate VT chamber (see Figure S14) and consisted of 48 turns per side. The ^{13}C detection coil was wound on a thin sheet of FR4 fiberglass wrapped around the 2 in. diameter reactor and consisted of 108 turns per side. The tuning and matching for each channel was achieved with fixed C22CF series chip capacitors (Dielectric Laboratories, Cazenovia, NY) used in parallel with variable capacitors (model 5601, Johanson, Boonton, NJ). The ^{1}H tuning capacitance C_T = 150 + 82 + 0-30 variable pF with matching capacitance C_M = 82 + 220 pF. Similarly, for the ^{13}C channel C_T = 680 pF and C_M = 1000 + 271 pF. Adjustment of ^{1}H B_1 frequency is set according to $B_{1,1H} = B_{1,13C} \cdot \gamma_{1H}/\gamma_{13C}$ with the variable tuning capacitor. Measurements were taken with an Agilent 4263B LCR meter with a 16334A test fixture at 100 Hz or with an Agilent E5071C network analyzer using a compensated cable. Later the ^{1}H and ^{13}C frequencies were changed to 246.6 and 62.0 kHz respectively with very minor changes in Q and match. The 300 ppm B_0 inhomogeneity of the electromagnet results in a required excitation bandwidth of the RF coil of 74 Hz for ^{1}H at 246.6 kHz and 18.5 Hz for ^{13}C at 62 kHz. Despite the relatively high Q of the coils (for the frequency), these bandwidths were easily achieved as seen by the coil bandwidths reported in Table S1. As described later below, the calibrated RF pulse durations were set to yield approximately twice the coil bandwidths in order to cover any spin system manipulation inefficiencies arising from B_0 and B_1 inhomogeneities (Figure S2 and Figure S3).

Table S1. RF Probe Channel Temperature Dependence

	TC = Room Temperature (22 °C)		TC = 60 °C	
	^{1}H	^{13}C	^{1}H	^{13}C
B_1 (kHz)	244.88	61.55	244.65	61.5
Q (at 3 db)	43.7	35.1	41.9	33.5
Match (dB)	-20.7	-18	-26	-21
Bandwidth (kHz)	5.61	1.752	5.841	1.835

TC refers to the temperature of the coil.

RF pulse calibration of multi-channel RF probes in instrumentation involving electromagnets for generating the B_0 field is commonly performed with water with the field strength set for proton resonance at the desired frequency. Such a procedure was performed here to calibrate the RF pulses for protons at 246.6 kHz and, indirectly, ^{13}C at 62.0 kHz in accord with a referencing scheme[4,5] previously reported for this hyperpolarizer.[2] The calibration phantom consisted of a hollow polypropylene sphere filled with 52 mL of water doped with 5 mM $CuSO_4$ to reduce spectroscopic repetition time T_R.

A pulse sequence available with the NMR spectrometer software Prospa (Magritek, Wellington, New Zealand) for obtaining a nutation curve at fixed power (i.e. 1Pulse Duration Sweep) was used to obtain directly (as supplied by the manufacturer) RF flip angle calibration curves for the PHIP probe RF channels resonant at 246.6 kHz and 62.0 kHz (Figure S3). At 246.6 kHz 8 averages per data point in the nutation curve were used, whereas at 62.0 kHz the number of averages per point was increased to 128 to increase the SNR. Following collection the signal model $sig_r(k) = A_r \cdot e^{\alpha k} \cdot \cos(w_r k + p_r)$ was fitted to the noisy nutation data. According to the fitted model, $t_{90°}$ ~ 100 µs for protons resonant at 246.6 kHz when using 2.5 W of power and $t_{90°}$ ~ 70 µs for protons resonant at 62.0 kHz with 0.6 W of power. The ^{13}C pulse length (at the same 62.0 kHz resonant frequency) was then calculated from water according to $T_{90,1H} \cdot \gamma_{1H}/\gamma_{13C}$ where γ_{1H} = 42.576 MHz/T and γ_{13C} = 10.705 MHz/T, yielding an estimated $t_{90°}$ ~ 280

μs for ^{13}C at 62.0 kHz. Using the same power settings for each channel as before, ^{13}C $t_{90°}$ was calibrated afterwards with hyperpolarized material to ~ 295 μs with $t_{180°}$ being measured as 540 μs. That the ratio $t_{180°}/t_{90°}$ for ^{13}C is not an integer multiple is attributed to: (i) RF coil efficiency differences for the large water phantom compared to the much smaller HP ^{13}C-labelled material in the reactor; and (ii) observed irregularities in the hard pulse waveform (and hence pulse power) on an oscilloscope due to running 250 W RF amplifiers (model BT00250-AlphaS, Tomco Technologies, Stepney, South Australia) at very low power levels, and (iii) others.

In addition to their use for calibrating RF flip angles, the nutation curves in Figure S3 also permitted measuring the overall B_1 homogeneity for each PHIP probe channel. At 246.6 kHz, the proton coil B_1 homogeneity as determined by the ratio of signal intensity for a 450° flip angle pulse versus a 90° pulse was measured as 0.78. Similarly for ^{13}C (using water) resonance at 62 kHz, B_1 homogeneity was measured as 0.91.

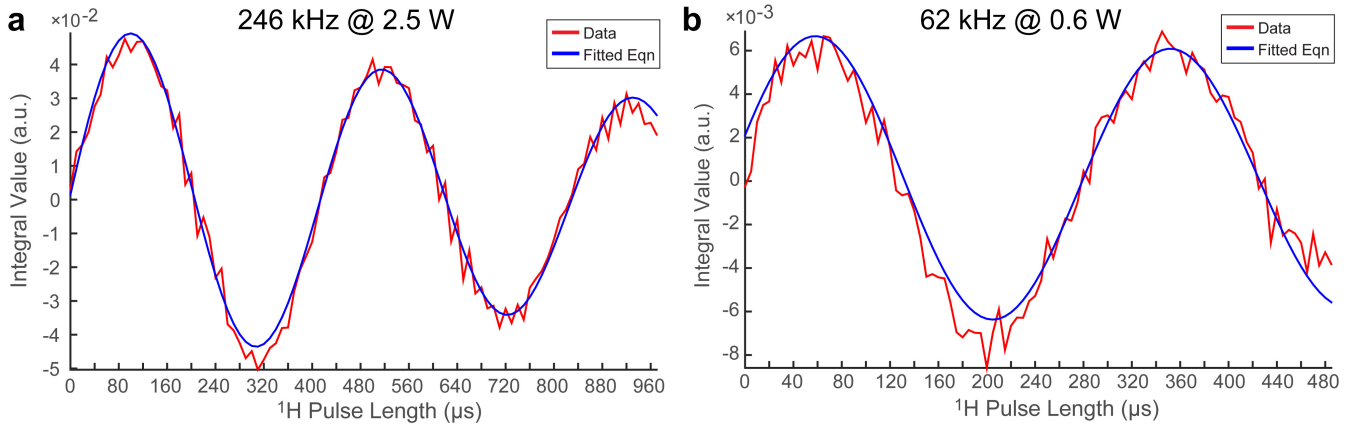

Figure S3. RF pulse calibration nutation curves. A 52 mL spherical polypropylene phantom filled with 5 mM $CuSO_4$ doped water was used to calibrate the RF pulses for proton and ^{13}C resonance frequencies at B_0 = 5.75 mT. (a) Fitting of signal model $sig_r(k) = A_r \cdot e^{\alpha k} \cdot \cos(w_r k + p_r)$ to the noisy proton nutation data yielded $t_{90°}$ = 100 μs for protons at 246.6 kHz, whereas $t_{90°}$ = 70 μs for protons at 62.0 kHz (b) yielded an estimated $t_{90°}$ ~ 280 μs for ^{13}C at 62.0 kHz.

4. HCA Preparation Using RF-based Approach: Experimental Polarization Transfer Sequence Parameters

HP 1-^{13}C-succinate-d_2 (SUX) contrast agent was produced using the Goldman polarization transfer sequence[6] and HCA preparation steps reported in Ref. #4. Rh(I)-based molecular catalyst[7,8] in aqueous medium was prepared in accord with a previously developed protocol[9] with further details of the catalyst preparation steps given in Ref. #10. The 1-^{13}C-fumaric acid-d_2 substrate (PHIP precursor) concentration was 30 mM, and the Rh(I) catalyst concentration was ~5.3 mM. HP 1-^{13}C-succinate-d_2 was produced inside the PHIP hyperpolarizer, and tested for percent ^{13}C polarization *in situ*, i.e. quality assurance (QA), using a 30° RF excitation pulse.

HP 1-^{13}C-phospholactate-d_2 (PLAC) was produced using the protocol described in Ref # 11. The evaluation of 1-^{13}C-phosphoenol-pyruvate-d_2 (1-^{13}C-PEP-d_2 or PEP) hydrogenation (Figure S7b) was used in HP studies: approximately~25 mM solution of 1-^{13}C-PEP-d_2 ([PEP]/[Rh(I)] > 6.5:1) with 30 mM phosphate buffer in D_2O was prepared at pH = 10.3 for subsequent use with PHIP hyperpolarizer. Temperature probe was placed on the surface of the reactor monitoring its temperature. Typical reactor temperature was ~55-60 °C. The Goldman[6] spin order transfer sequence was employed

for all polarization transfer for production of HP SUX and HP PLAC. Figure S4 provides the detailed information about the efficiency of polarization transfer for HP SUX and HP PLAC production as a function of t_1 and t_2 timings. See the main text for additional discussion and correlation with SUX theoretical study.[12]

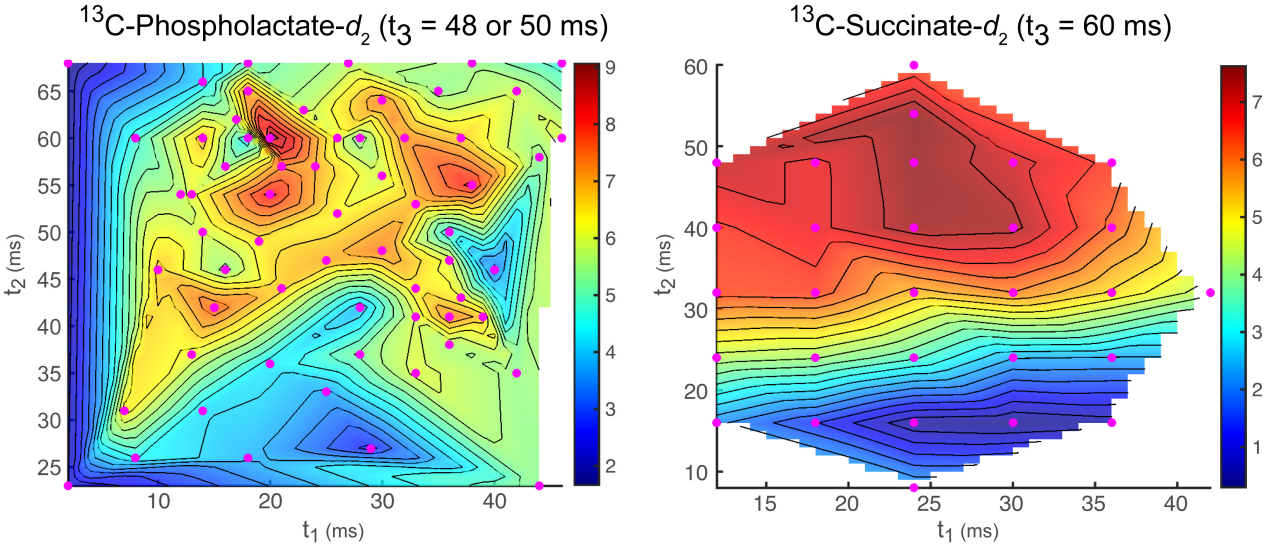

Figure S4. HCA experimental Goldman polarization transfer sequence timing delay maps. (left) With t_3 held at 48 or 50 ms (negligible difference between the timings), ^{13}C signal levels for 1-^{13}C-phospholactate-d_2 (PLAC) were obtained for varying t_1 and t_2 timing delays at the points indicated (magenta). Similar testing was performed with 1-^{13}C-succinate-d_2 (SUX) (right). The signal levels shown in the plots are from magnitude spectra.

5. MRI Imaging of HP ^{13}C-PLAC Imaging and Voxel-Based HCA Kinetics

The ^{13}C images acquired at 4.7 T using HP ^{13}C-PLAC contrast agent are shown in Figure S5 without the interpolation (32×32 to 1024×1024 matrix size) used in the Main Text for Figure 7. For the mouse heart, the slice in Figure S5a (left panel) contained the voxels with the highest recorded intensity during the time-course of successive image acquisitions post-tail vein injection. The six most intense voxels of this slice were ordered according to their intensity. These voxels' intensities were then tracked across all the successive image acquisitions (~4 s between successive images) by Fourier transforming the image acquisition k-space data, adding the chosen slice from each acquisition to an image stack in MATLAB (i.e. time dimension), and then extracting from the stack the time-course of the six chosen voxels. The ^{13}C HP PLAC/LAC kinetics in the heart delineated by the mapped time-course of these tracked voxels are shown in Figure S6. Production of PLAC hyperpolarization was $\%P_{13C}$ = 2.7 ± 0.5% for this representative *in vivo* experiment.

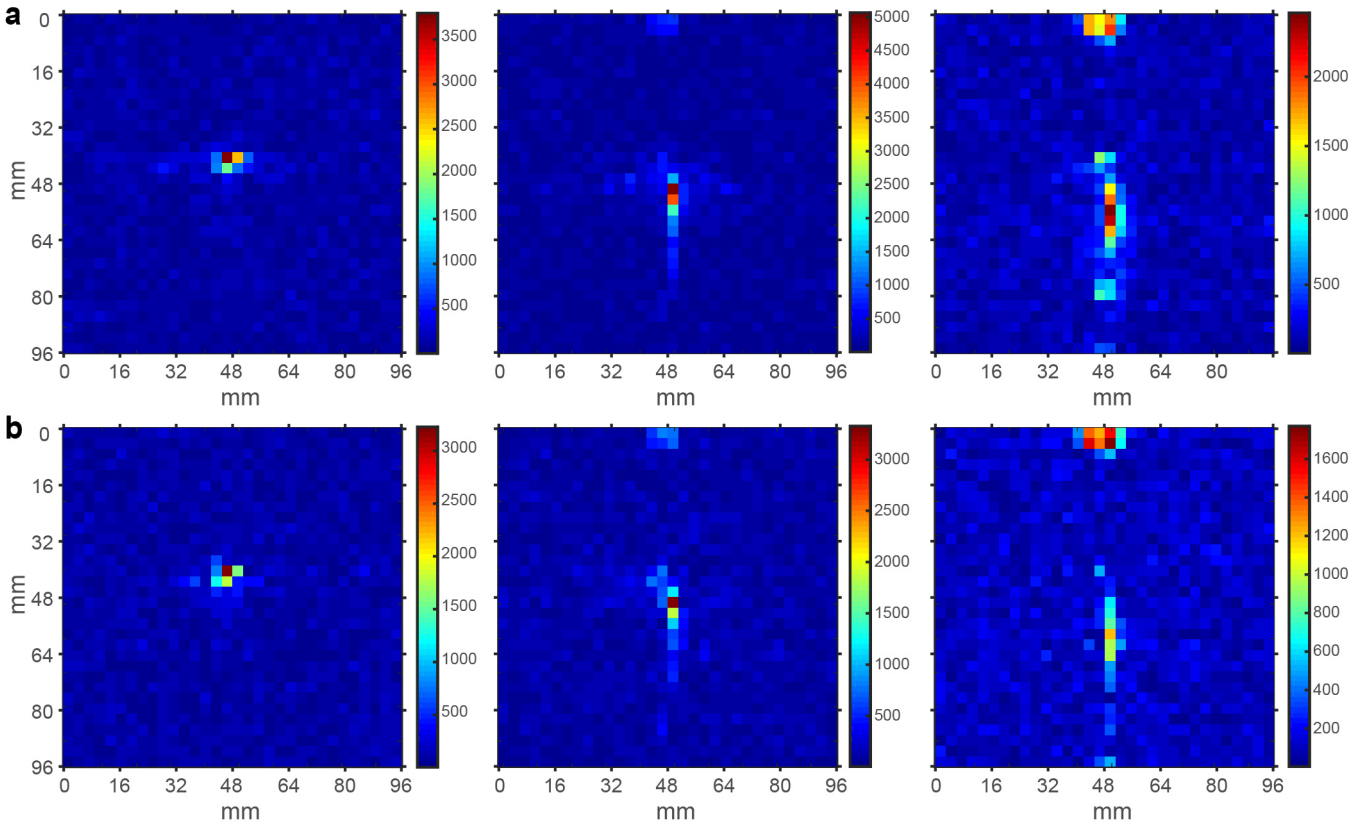

Figure S5. *In vivo* PLAC raw ^{13}C images. Imaging matrix 32×32 with FOV of 96×96 mm^2 acquired at 4.7 T shown without the additional processing (interpolation) used in the Figure 7 (main text). The two 6 mm slices are otherwise as previously described (see Main Text Figure 7).

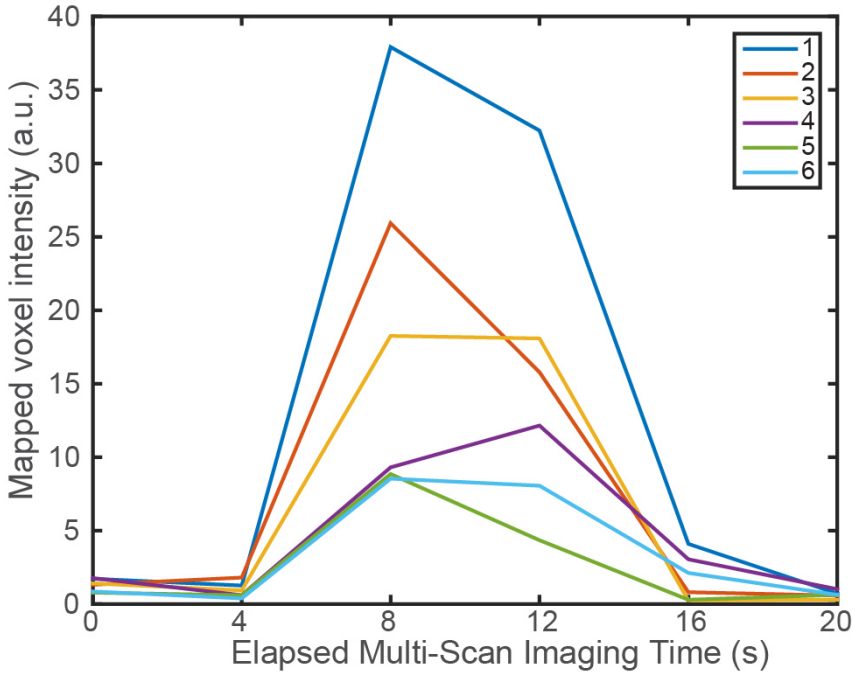

Figure S6. *In vivo* mouse heart PLAC kinetics. The wash-in and wash-out kinetics of HP PLAC in a healthy mouse heart obtained from tracking voxel intensity variation across multiple imaging scans is shown for the time-course of the 6 most intense voxels from the left image of Figure S5a.

6. *In Operando* Dynamics of HCA Production

In the context of the particular physical configuration of the 5.75 mT PHIP hyperpolarizer described in this work, variables affecting the reaction kinetics and polarization yield were investigated. First, advantage was taken of heat production by the electromagnet to additionally regulate the temperature of the chemical reactor by modulating the magnet temperature via speed control of external cooling fans. A two-meter length of 1/8 in. PTFE tubing wrapped around the PHIP probe body inside the magnet created the injection-heating loop (Figure S1). Two parameters of the PHIP polarization process were optimized: pre-injection delay and hydrogenation time in the reactor. Continuous wave (CW) proton decoupling was applied during the entire hydrogenation time. The pre-injection time allows increase the reagent temperature prior to spraying the solution into atmosphere of *para*-H_2 gas. It was found that pre-injection delay of ~1.0 second is optimal (Figure S7a) for HP SUX production. The injection delay of 5±1 seconds was found optimal for production of HP SUX and HP PLAC (Figure S7b).

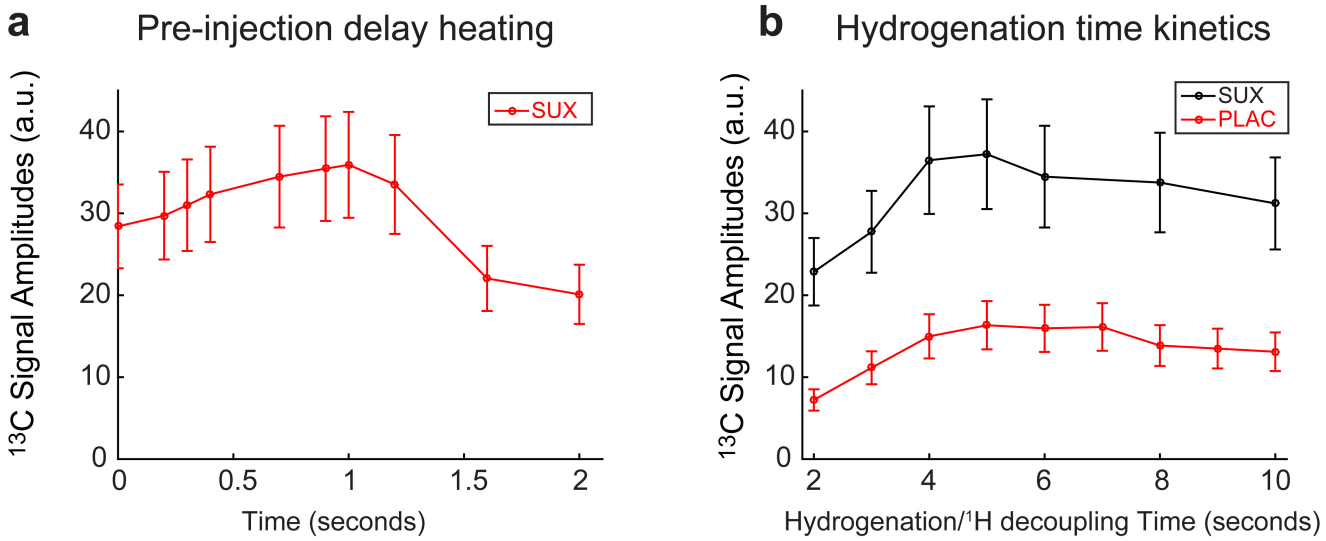

Figure S7. HCA reaction kinetics. (a) Kinetics of the catalyst and precursor molecule observed via *in situ* detection of ^{13}C signal versus the pre-injection delay time where the precursor is allowed to warm within the heating loop for the specified delay time. (b) Hydrogenation/^{1}H decoupling time analysis of the precursor molecule for the optimum pre-injection delay of ~1.0 s.

7. Additional Technical Drawings

Reactor Bottom Cap

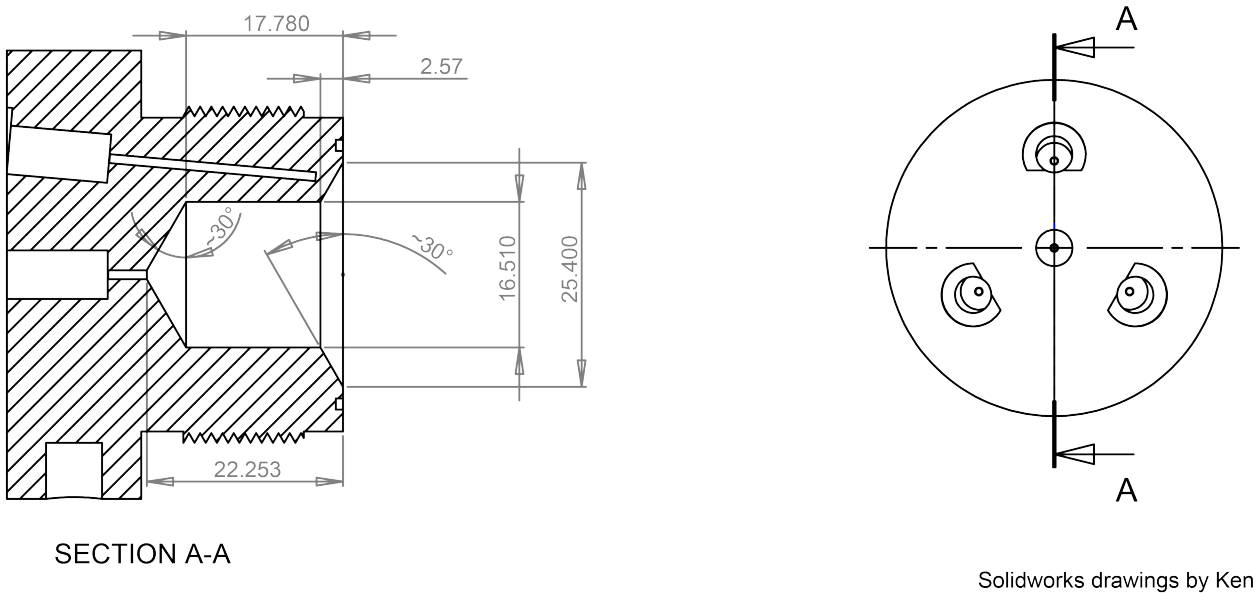

Solidworks drawings by Ken Wilkens

Figure S8. Bottom cap drawings for reactor. Dimensions are in mm. This component is made from 2 in. OD stock of polysulfone rod.

Reactor Top Cap

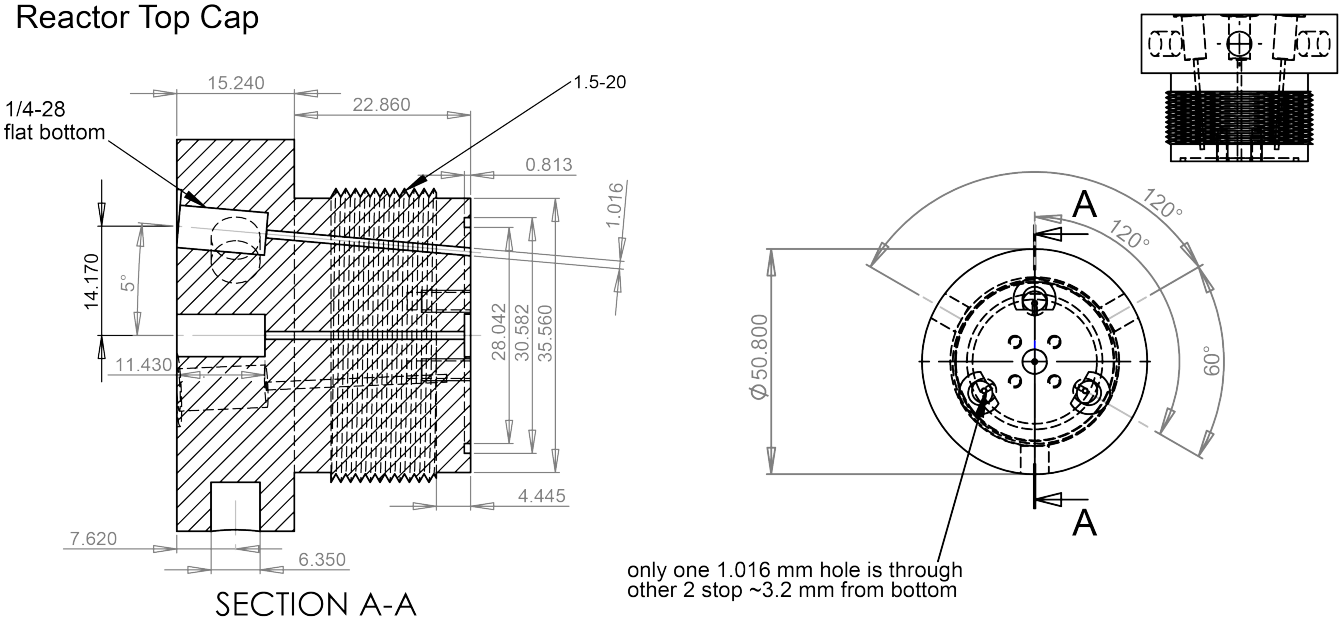

Solidworks drawings by Ken Wilkens

Figure S9. Top reactor cap drawings. Dimensions are mixed in mm and inches. This component is made from 2 in. OD stock of polysulfone rod.

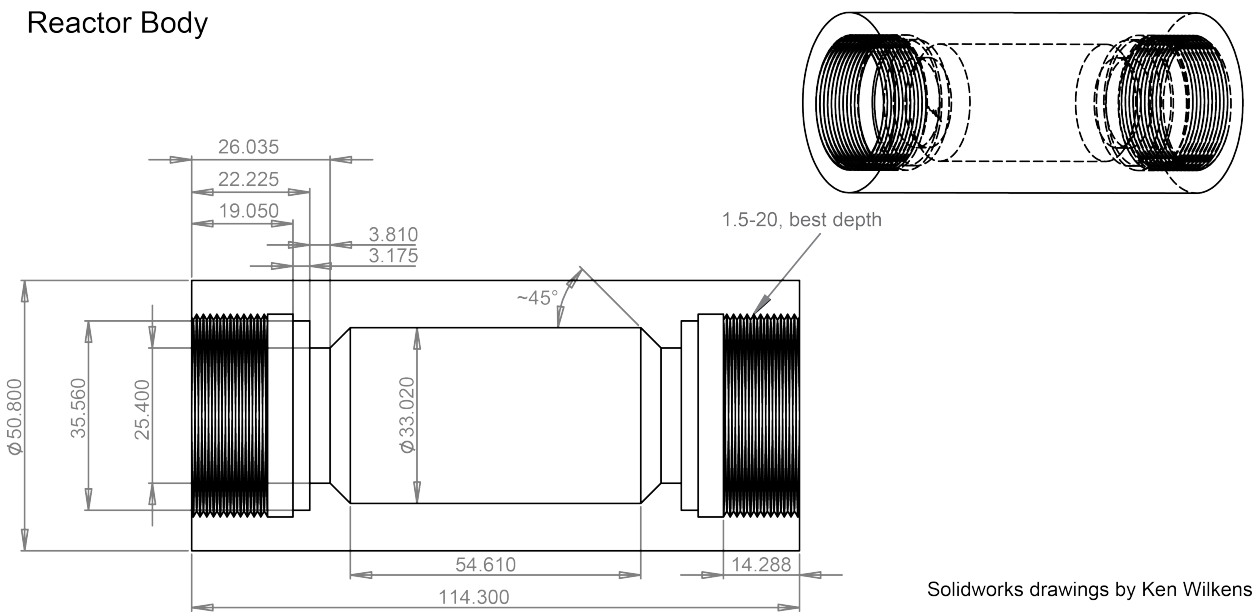

Figure S10. Drawings for the PHIP polarizer reactor body. Dimensions are mixed in mm and inches. Two O-rings (1 mm thick, 28 mm ID, made of BUNA material, P/N 9262K625 from McMaster-Carr) are placed inside this part for providing gas-tight seal, when connecting this part with reactor top and bottom caps (Figure S8 and Figure S9 respectively). This component is made from 2 in. OD stock of polysulfone rod.

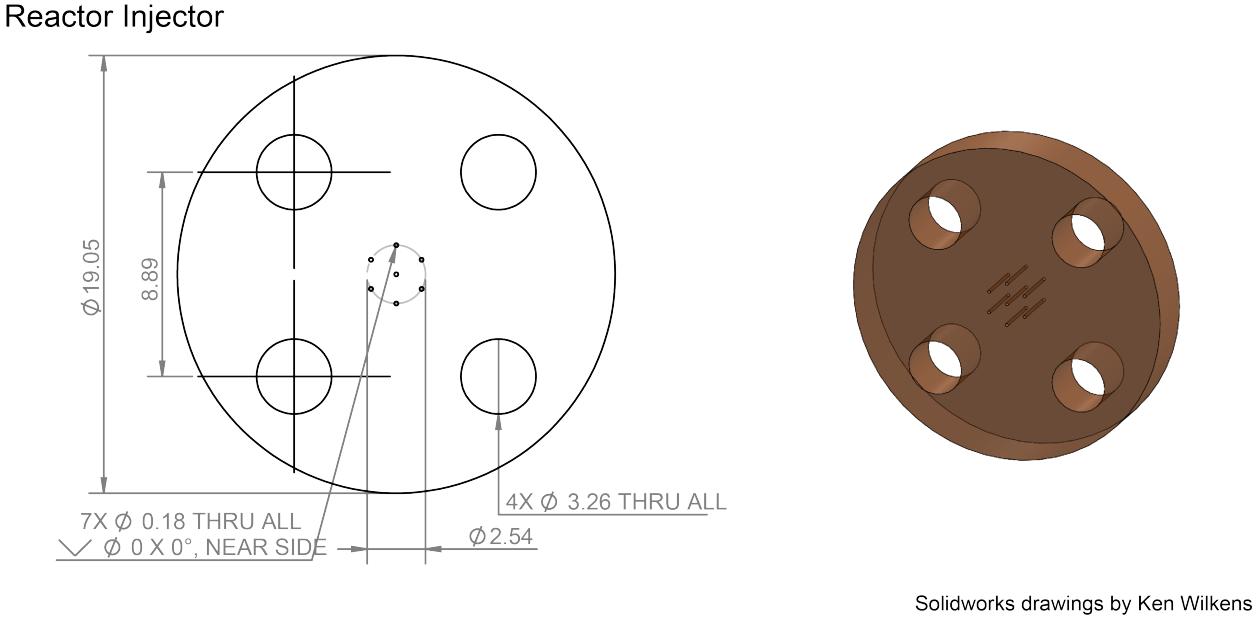

Figure S11. Drawings for injector for reactor. Dimensions are in mm. The injector mounts to the reactor top cap (Figure S9) using four nylon screws and the O-ring (1 mm think, 4 mm ID, BUNA material, P/N 9262K102 from McMaster-Carr). The cluster of 7 holes is not drilled all the way through. Instead, it is finalized with micro-drill manually resulting in ~0.25±0.05 mm hole. The cluster of seven holes provides a convenient means of spray injection. It is robust, because even if partial clogging of one or more injector holes occurs the device can continue function without disruption (arguably as somewhat reduced performance). Moreover, this part is disposal, and when the reactor is being cleaned (from residual Rh deposits), a new spray injector is installed. This component is made of polysulfone.

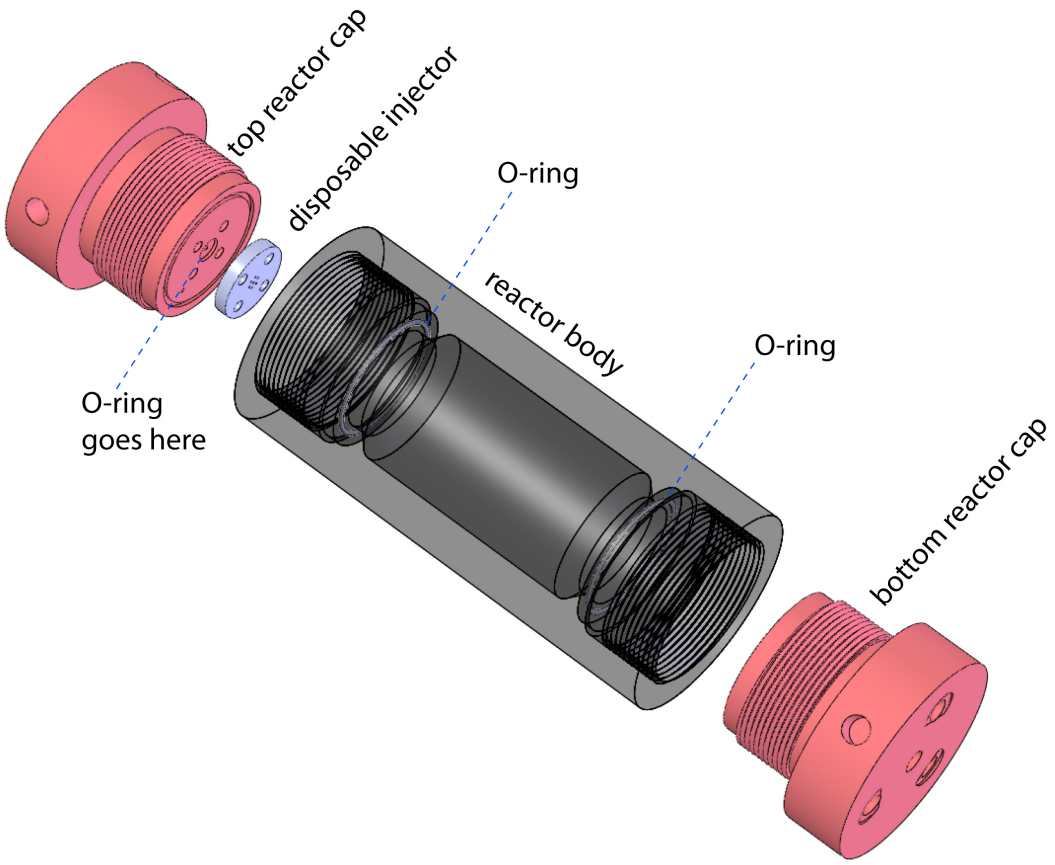

Figure S12. Technical drawing showing the connection/assembly of the reactor components. All components are made of polysulfone except for two O-rings. See the figures above for the specific details.

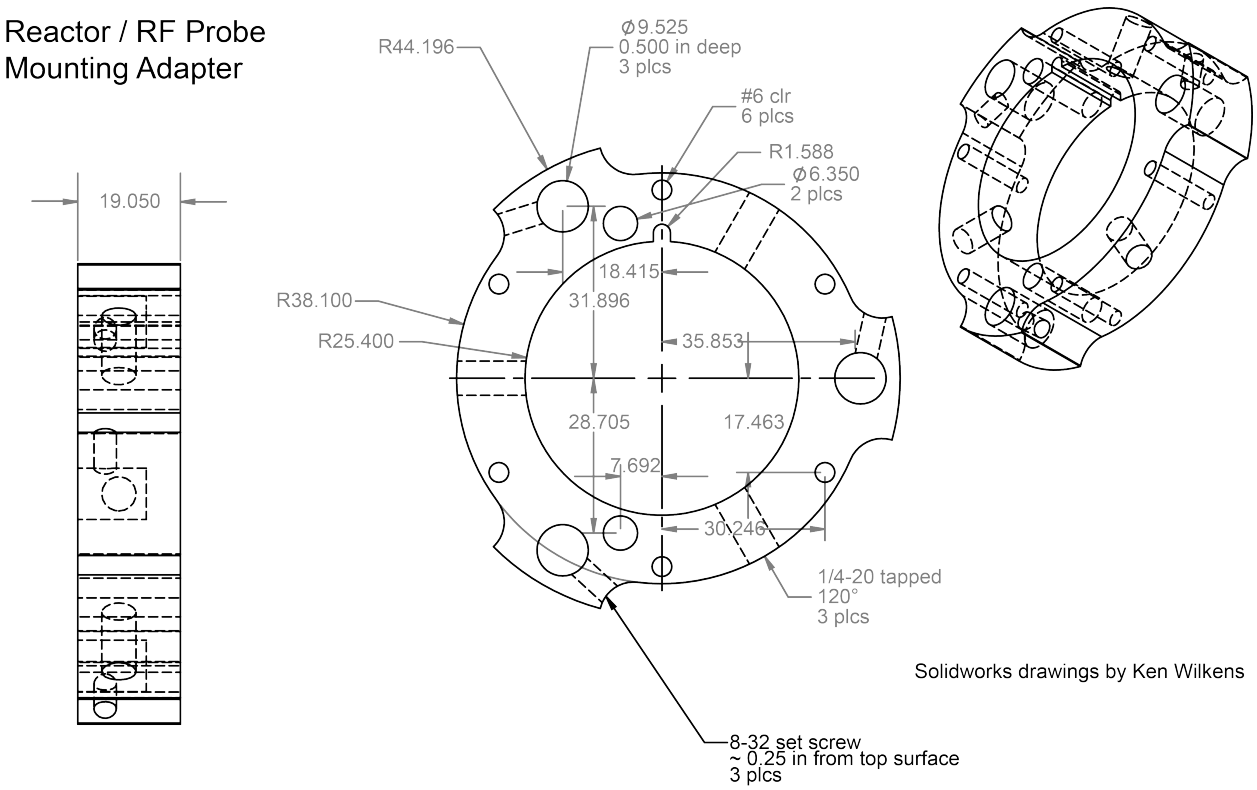

Figure S13. Drawings for mounting adapter for reactor and RF probe connections. Dimensions are mixed in mm and inches. The top reactor top cap (Figure S9) is used for mating with this component using set-screws. Dimensions are mixed in mm and inches.

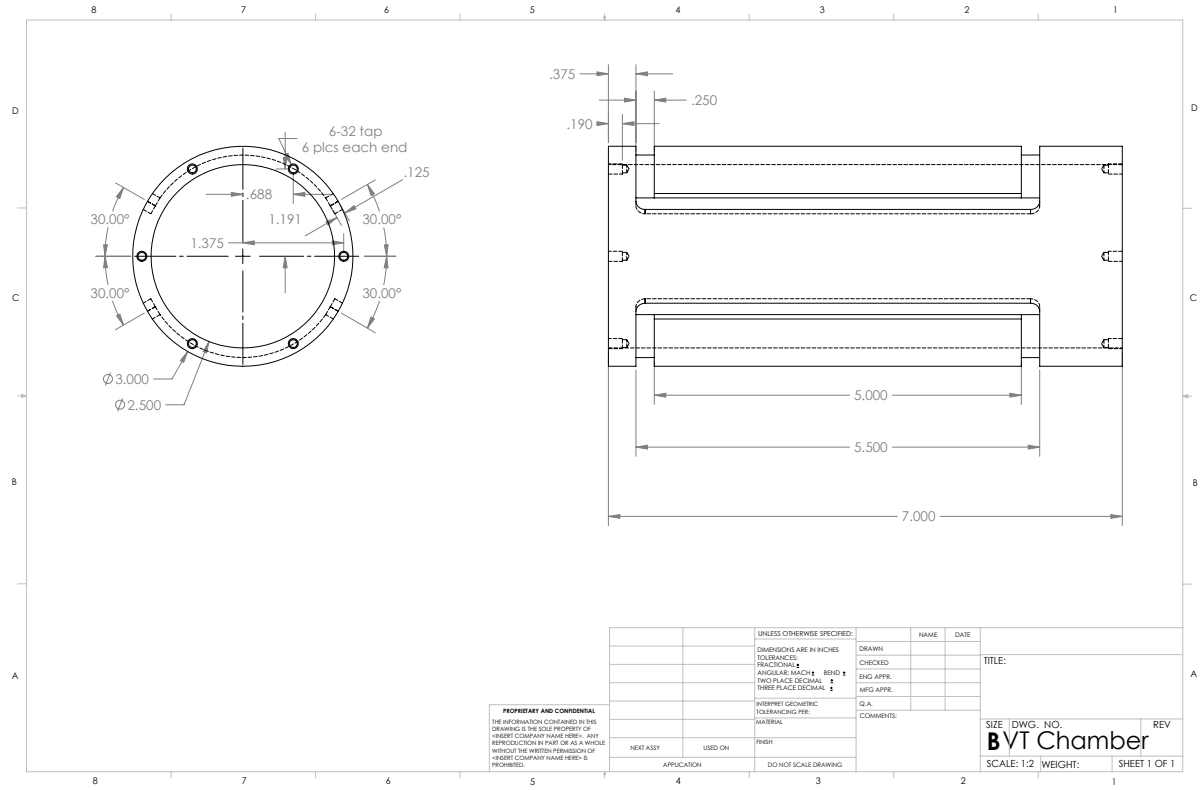

Figure S14. Drawings of variable temperature (VT) chamber body enclosing the reactor. This component is made of acrylic. This component also serves as a placeholder/guide for the ^{1}H RF coil at 246 kHz. The turns of the coil are placed inside of the grooves. Dimensions are mixed in inches.

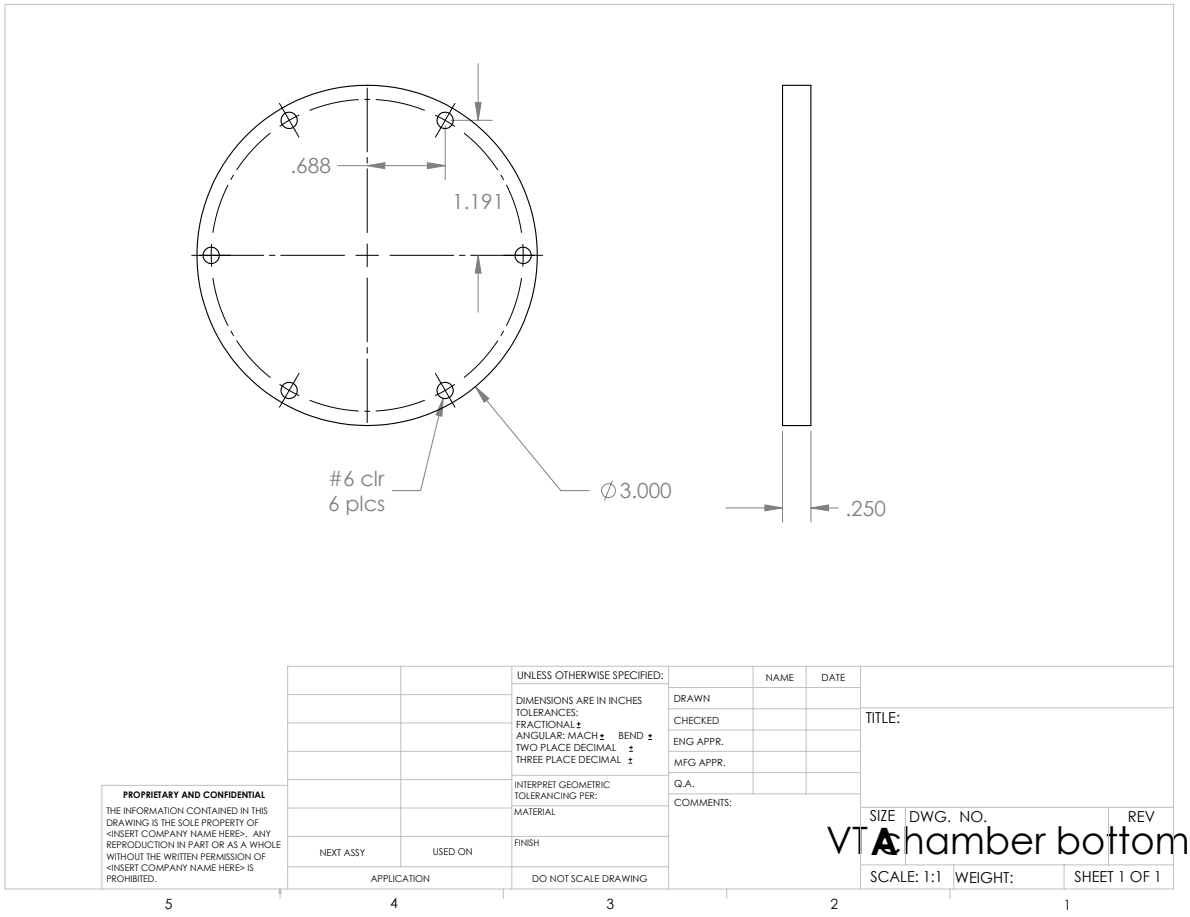

Figure S15. The drawing of variable temperature (VT) bottom cap. This component is made of polysulfone material, but can be made of other plastic materials too. Dimensions are mixed in inches.

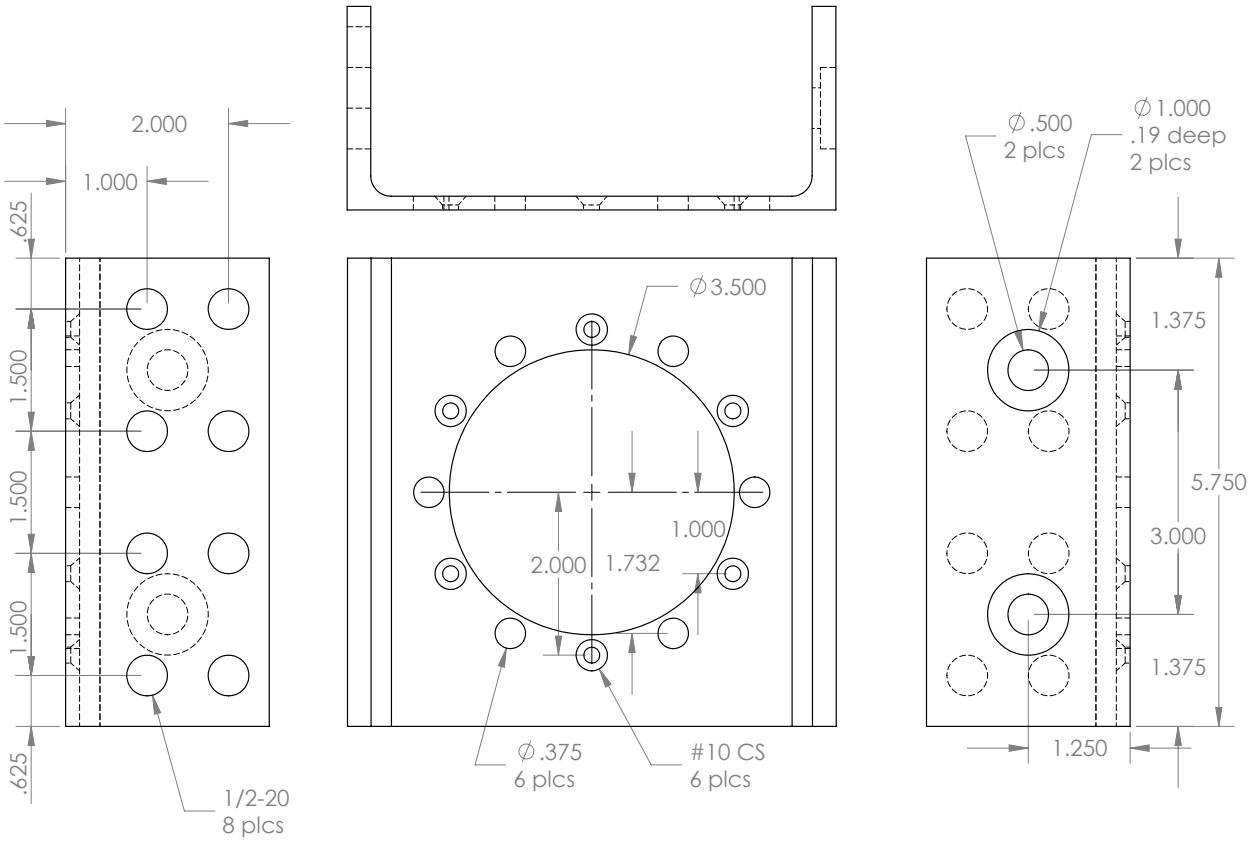

Figure S16. The drawing of the RF probe base component made of aluminum U-channel. Dimensions are mixed in inches.

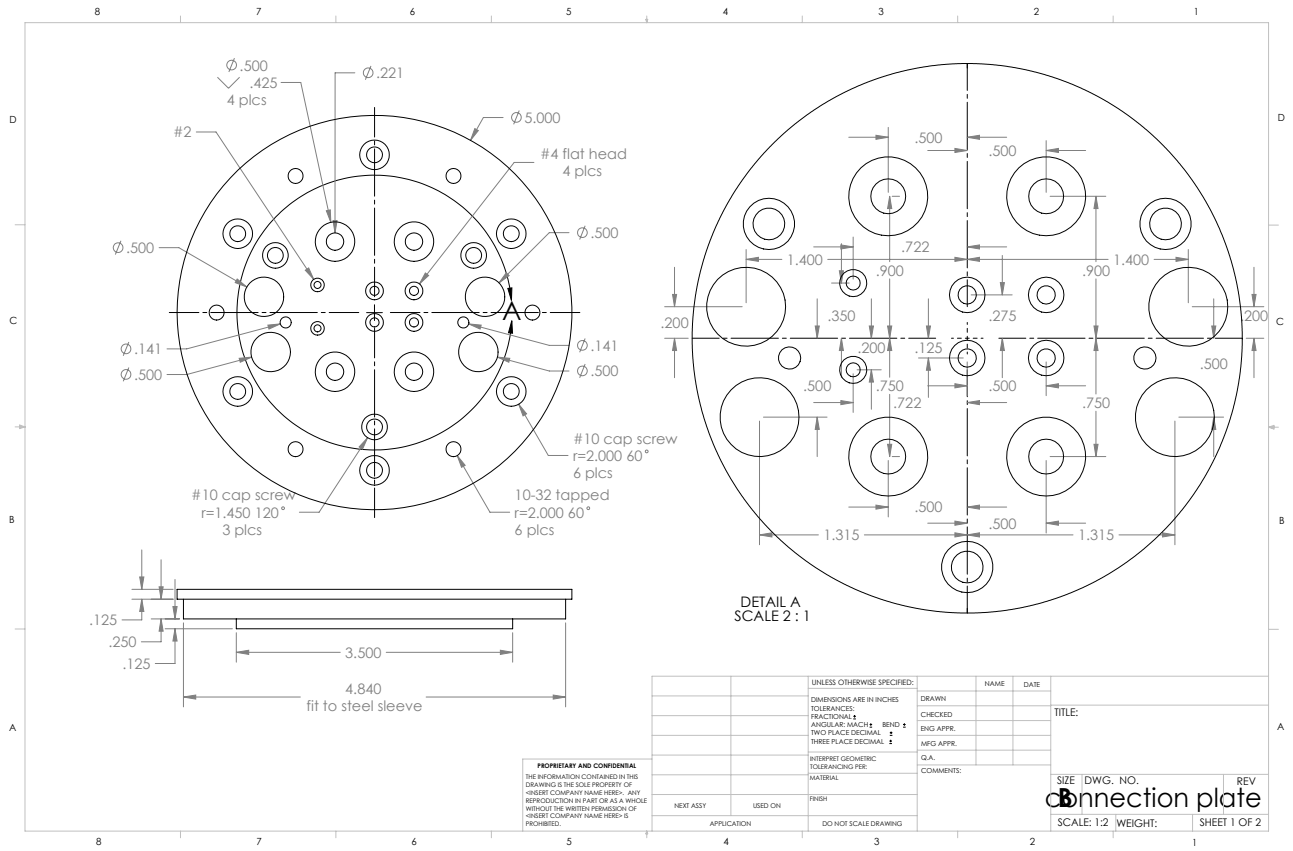

Figure S17. The drawing of the copper connection plate used to connect RF probe base. Note four 0.5 in. through holes built for placing the wave-guides. Dimensions are mixed in inches.

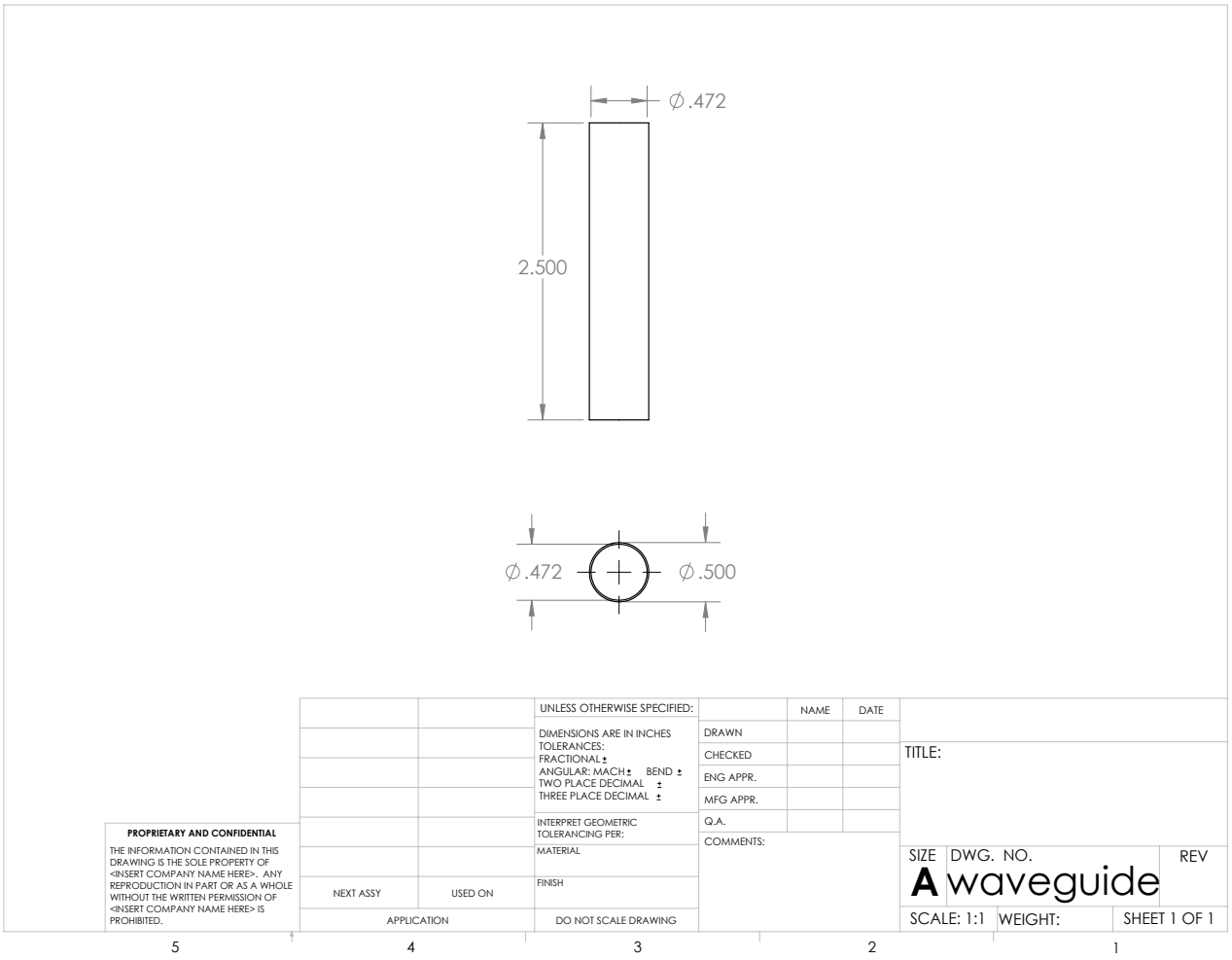

Figure S18. The drawing of the wave-guide made of brass tubing. This part is machined from the stock material: P/N 8859K33, McMaster-Carr. Dimensions are mixed in inches.

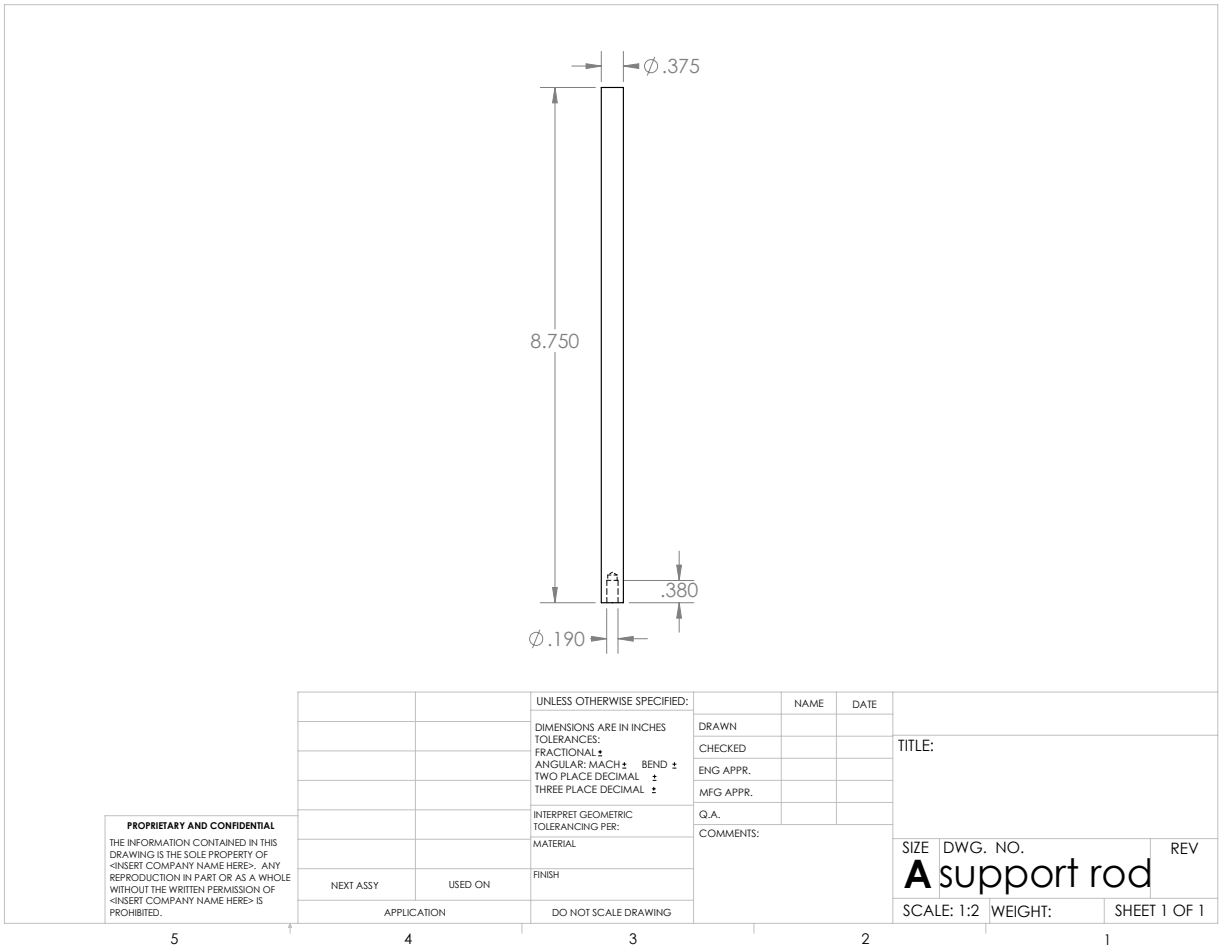

Figure S19. The drawing of the FR4 fiberglass mounting rods (3 pcs). Dimensions are mixed in inches.

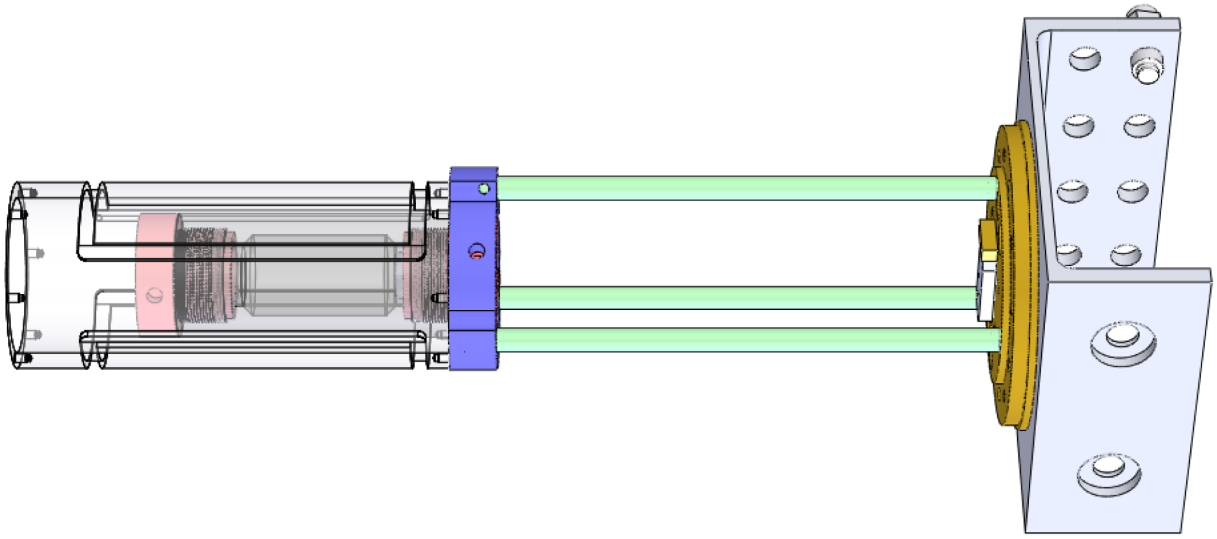

Figure S20. The overall design of the dual-channel RF probe showing how the individual components are connected. The support rods (shown in green) are made of 0.5 in. diameter fiberglass material (for more information see above text). The length is adjusted to accommodate the reactor in the B_0 center isocenter. This drawing shows the overall assembly of the reactor, variable temperature (VT) chamber and other components.

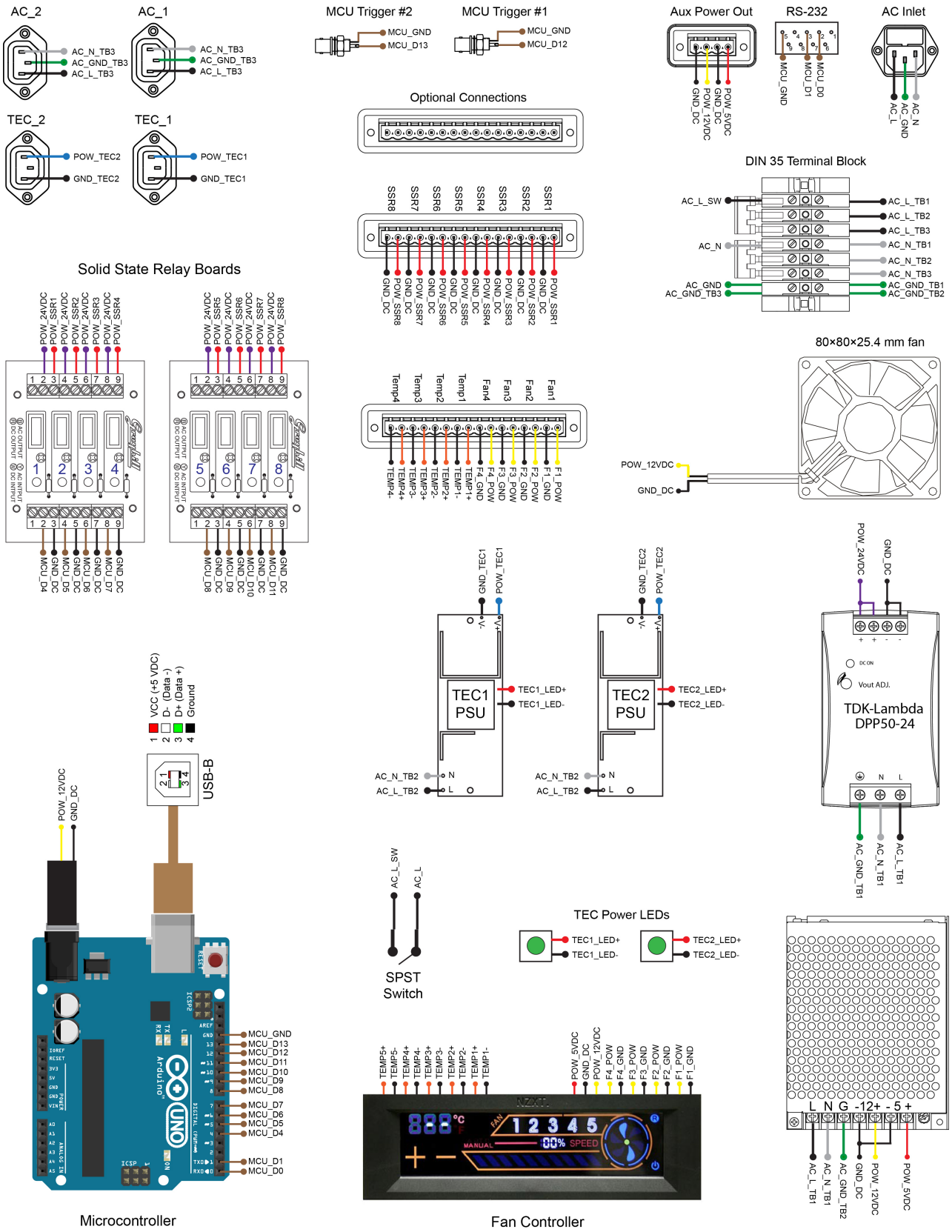

Figure S21. PHIP controller unit schematic.

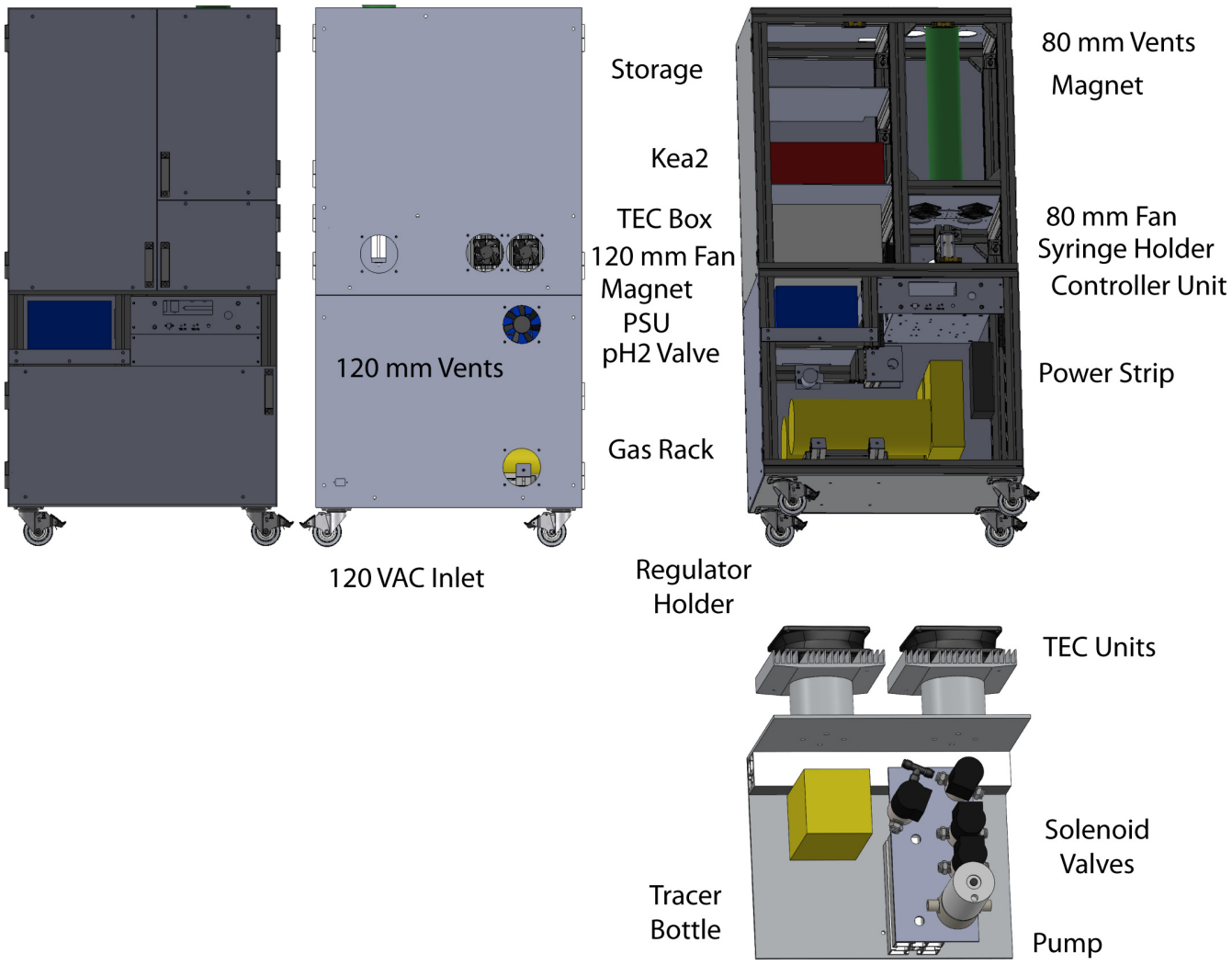

Figure S22. The alignment of components in the PHIP hyperpolarizer frame.

9. Animal Experiments

Rats. Female Spraque Dawley rats (8 weeks old, n=5) (Charles River) were anesthetized with a mixture of 200 µL ketamine:xylazine (50mg/kg:8mg/kg) via intraperitoneal injection. Then, a 26-G needle attached to a catheter was inserted into the lateral tail vein while the animal lying on an MRI coil holder. The animal was placed inside the RF coil of 0.0475 T portable MRI scanner, the bore of which (~35 °C) conveniently provided warm environment for the animal during NMR scan. Prior to acquiring the non-localized ^{13}C NMR spectra, the animal (Figure 6c) were injected with ~1 mL of hyperpolarized agent (HP SUX) via the catheter within 5 seconds. After NMR spectroscopy (~2 minutes), animals were removed from the scanner and retrieved in a warm cage under constant observation. The anesthetic dose was designed to immobilize animals for approximately 45 minutes.

Nude mice. Mouse model of breast cancer (10 weeks old, n=6). Murine breast cancer cell lines (mammary epithelial tumor cell line) C57MG were cultured and maintained in Dulbecco modified Eagle medium (Mediatech, Manassas, VA) in the presence of 10% fetal calf serum (FCS; Invitrogen, Carlsbad, CA), penicillin-streptomycin antibodies (Mediatech), and 10 µg/ml insulin (Sigma-Aldrich, St Louis, MO) at 37°C and 5% CO_2 incubator. We generated an orthotropic mouse model of breast cancer by injection of C57MG cells in the fat pad of nude mice. The imaging commenced when the tumor size became palpable or approximately 0.4 cm. The mice were anesthetized using ketamine:xylazine (75mg/kg: 5mg/kg) via intraperitoneal injection. Then, a 28-G needle attached with a catheter was inserted in the lateral tail vein while the animal lying on the MRI coil holder. Prior to acquiring NMR spectroscopy or MRI imaging, animals were injected with ~0.2 mL of hyperpolarized contrast agent (HP PLAC) via the catheter within 5 seconds. After imaging, animals were removed from the scanner and retrieved in a warm cage under constant observation. The anesthetic dose was designed to immobilize animals for approximately 60 minutes.

Table S2. Miscellaneous PHIP polarizer chassis components.

Part Number	Description	Supplier	Purpose
N/A	6126 microfluidic solenoid valve	Burkert Fluid Control Systems	eject valve
98162798	PEEK base for 6126, 1/4-28F, custom	Burkert Fluid Control Systems	
5077T123	Submersible Stainless Steel Solenoid Valve, Fluoroelastomer Seal, 1/8 NPT Female, 325 PSI, 24 VDC	McMaster	precursor, vent, N_2 valves
48325K282	High-Pressure Stainless Steel Solenoid Valve, PTFE Seal, Normally Closed, 1/8 NPT Female, 24 VDC	McMaster	inject valve
1194N26	High-Pressure Hazardous-Location Stainless Steel Solenoid Valve, Pctfe Seal, for Gas, 24V DC, 1/4 Pipe Size, 1500 PSI	McMaster	*para*-H_2 valve
7864A11	Line Regulator, 0-60 PSI Operating Pressure, 0-60 PSI Gauge	McMaster	pressurize precursor bottle
5779K11	Straight Connector for 1/8" Tube OD	McMaster	plumbing
5779K31	Tee for 1/8" Tube OD	McMaster	plumbing
5239K23	Extreme-Temperature Tubing Made with Teflon® PTFE, 1/32" ID, 1/16" OD, 1/64" Wall, Semi-Clear White	McMaster	plumbing
5239K24	Extreme-Temperature Tubing Made with Teflon® PTFE, 1/16" ID, 1/8" OD, 1/32" Wall, Semi-Clear White	McMaster	plumbing
5779K102	Push-to-Connect Tube Fitting for Air, Straight Adapter for 1/8" Tube OD x 1/8 NPT Male	McMaster	plumbing
5779K243	Push-to-Connect Tube Fitting for Air, Straight Adapter for 1/8" Tube OD x 1/4 NPT Male	McMaster	plumbing
5779K11	Push-to-Connect Tube Fitting for Air, Straight Connector for 1/8" Tube OD	McMaster	plumbing
5779K31	Push-to-Connect Tube Fitting for Air, Tee for 1/8" Tube OD	McMaster	plumbing
9262K102	Multipurpose O-Ring, Oil-Resistant Buna-N, 1mm Wide, 4mm ID, packs of 100	McMaster	reactor injection seal
9262K624	Multipurpose O-Ring, Oil-Resistant Buna-N, 1mm Wide, 25mm ID, packs of 100	McMaster	reactor seal
93135A106	Nylon Pan Head Machine Screw, Slotted, 4-40 Thread, 1/4" Length, packs of 100	McMaster	reactor screw
55165A38	Metric Fixed Pin Spanner Wrenches for Holes for 52 to 55mm Circle Diameter, 5mm Pin Diameter, 5/32" Long Pin	McMaster	reactor assembly tool
92421A194	Brass Knurled Head Thumb Screw with Flared Shoulder, 8-32 Thread, 1/2" Long, packs of 25	McMaster	chassis valve plate fitting
1939K13	DC Equipment Cooling Fan, 3.15" Square x 1.26" Depth, 31 CFM, 12 VDC	McMaster	cooling system

1939K25	DC Equipment Cooling Fan, 4.69" Square x 1.5" Depth, 105 CFM, 12 VDC	McMaster	cooling system
19155K36	EMI/RFI Fan Guard for 3.15" (80 mm) Fan	McMaster	cooling system
19155K38	EMI/RFI Fan Guard for 4.69" & 4.72" Fans	McMaster	cooling system
19155K44	Plastic Fan Guard for 3.15" (80 mm) Fan	McMaster	cooling system
19155K46	Plastic Fan Guard for 4.69" & 4.72" Fans	McMaster	cooling system
9452K116	Oil-Resistant Buna-N Multipurpose O-Ring, 1/16 Fractional Width, Dash Number 029, packs of 100	McMaster	precusor bottle seal
51025K211	Brass & Nylon Push-to-Connect Tube Fitting, Through-Wall Straight Connector for 1/8" Tube OD	McMaster	precursor bottle fitting
4061T118	Square-Profile O-Ring, Oil-Resistant Buna-N, Dash Number 013, packs of 100	McMaster	precursor bottle thru-wall seal
7330K64	Interference Limiting 8-Outlet Metal Surge Suppressor Outlet Strip	McMaster	power distribution
7330K64	Interference Limiting 8-Outlet Metal Surge Suppressor Outlet Strip	McMaster	power distribution
507-1235-ND	FUSE GLASS 10A 250VAC 5X20MM	Digikey	power distribution
Q212-ND	CONN AC RECEPT SCREW/.250 FO	Digikey	power distribution
150SP24-250	Bio-Chem Valve self-priming micro pump. 24 volt 250uL dispense volume.	Western Analytical	precursor dispensing pump
2333	CONNECTOR 1/4-28F 1/16in PEEK	Western Analytical	plumbing
P-703	Union Assy PEEK .050 thru 1/8	Western Analytical	plumbing
U-510-01	Adpt Body PEEK 1/8NPTx1/4-28F	Western Analytical	plumbing
U-500-01	Adpt Body PEEK 1/4NPTx1/4-28F	Western Analytical	plumbing
P-300X	Flangeless Ferrule 1/8in	Western Analytical	plumbing
008CZ16	OMNI-LOK INVERTED CONE ETFE 1/16in	Western Analytical	plumbing
XP-206	Flngls Sys Blue Delr 1/16in	Western Analytical	plumbing
XP-306	Flngls Sys Blue Delrin 1/8in	Western Analytical	plumbing
P-713	Tee Assy 1/8in PEEK .050 thru	Western Analytical	plumbing
XP-130	Flngls Sys Nat PEEK 1/8in	Western Analytical	plumbing (micro pump)
B0036WTDHK	SilverStone 120mm Fan Filter with Grill FF121 (Black)	Amazon	nifty fan cover alternative
B0040JHMHQ	SilverStone 80mm Fan Filter with Grill FF81B (Black)	Amazon	nifty fan cover alternative
N/A	misc custom RG316 SMB/BNC and SMA/BNC cables	Citrus Cables Inc	RF connections
89089-722	Corning 431430 150mL Storage Bottles, Square, Polycarbonate, Sterile	VWR	precursor bottle
MT101315-1	PHIP Chassis	Minitec Framing	hyperpolarizer framework

Table S3. PHIP hyperpolarizer controller unit bill of materials.

Part Number	Description	Vendor	Quantity	Price	Subtotal	Notes
MT101315-2	PHIP Controller Unit Enclosure	Minitec	1	400.00	400.00	current price
A24531-ND	CONN BNC JACK STR 50 OHM SOLDER	Digikey	2	3.18	6.36	
Q223-ND	CONN AC RCPT FMALE SCREW/.250 FO	Digikey	4	0.74	2.96	
277-6807-ND	CONN HEADER 16POS 5.08MM PNL MNT	Digikey	3	16.46	49.38	
277-6689-ND	CONN HEADER 4POS 5.08MM PNL MNT	Digikey	1	4.19	4.19	
277-3276-ND	FEED-THRU TERM BLOCK 24-12AWG	Digikey	7	2.82	19.74	Buying 9 suggested
277-2292-ND	END BRACKET FOR 35 MM DIN RAIL	Digikey	4	1.18	4.72	
277-3347-ND	TERM BLOCK INSERTION BRIDGE 3POS	Digikey	2	2.04	4.08	Buying 3 suggested
AFB0812VHB-F00	FAN AXIAL 80X25.4MM 12VDC WIRE	Digikey	1	12.65	12.65	
1053-1403-ND	FAN GUARD 80MM WIRE MESH BLACK	Digikey	1	1.50	1.50	
381-2344-ND	GRILL GRD FLTR&SPACR F/80MM FAN	Digikey	1	8.16	8.16	
MUSB-D511-00-ND	Connector Receptacle USB TypeB 2.0 4 Position Panel Mount, Through Hole	Digikey	1	10.06	10.06	
Q203-ND	CONN RCPT 5X20 FUSEHOLDER SCREW	Digikey	1	1.49	1.49	
626-1041-ND	D-Sub Connector Receptacle, Female Sockets 9 Position Free Hanging (In-Line) Solder Cup	Digikey	1	6.18	6.18	
102-2525-ND	AC/DC CONVERTER 5V 12V 60W	Digikey	1	38.93	38.93	
285-1219-ND	AC/DC CONVERTER 24V 50W	Digikey	1	54.54	54.54	
1175-1420-ND	CBL USB B MALE-OPEN END 2M BEIGE	Digikey	1	4.20	4.20	
277-2064-ND	DIN RAIL 35MMX7.5MM SLOTTED 1M	Digikey	1	9.82	9.82	
GH3031-ND	I/O MOUNTING BOARD G5 4POS	Digikey	2	34.10	68.20	
GH3040-ND	OUTPUT MODULE DC G5 13MA 5VDC	Digikey	8	13.98	111.84	
277-1493-ND	CONN TERM BLK END COVER	Digikey	2	1.32	2.64	
CP3-1000-ND	CONN 2.1MM FEMALE PLUG 5.5MM OUT	Digikey	1	1.36	1.36	
94865-01-ND	TERM FORK INSUL 22-18AWG #6	Digikey	10	0.26	2.59	
1050-1041-ND	ARDUINO UNO SMD REV3	Digikey	1	25.29	25.29	
507-1235-ND	FUSE GLASS 10A 250VAC 5X20MM	Digikey	1	0.22	0.22	
WM2948CT-ND	CONN QC RCPT 14-16AWG 0.250	Digikey	25	0.36	8.97	
S1231E-36-ND	CONN HEADER .100 SINGL STR 36POS	Digikey	2	3.90	7.80	
CW105-ND	SWITCH ROCKER SPST 10A 250V	Digikey	1	4.43	4.43	
350-1890-ND	LED PNL MT 9MM 6V BLACK GREEN	Digikey	1	7.42	7.42	Optional indicator for microcontroller status
36-7248-3-ND	HEX NUT 0.184" STN STEEL 4-40	Digikey	4	0.15	0.60	
36-7244-5-ND	JACK SCREW HEX 4-40	Digikey	2	0.57	1.14	
492-1074-ND	ROUND SPACER #4 NYLON 1/4"	Digikey	4	0.16	0.64	
B00PB0CFCA	Coca Cola 0.14 cubic foot Retro Fridge in Red	Amazon	2	44.99	89.98	disassembled for TEC, possible alternate of B000JLNBW4)
B002L16OMO	NZXT SENTRY 2 Accessories 5.25-Inch Touch Screen Fan Controller (Black)	Amazon	1	27.01	27.01	
93395A204	Type 316 Stainless Steel Flat-Head Socket Cap Screw, M3 Size, 10mm Length, .50mm Pitch, packs of 100	McMaster-Carr	1	10.53	10.53	

91771A155	18-8 Stainless Steel Flat Head Phillips Machine Screw, 6-32 Thread, 1-1/4" Length, packs of 100	McMaster-Carr	1	9.46	9.46
91771A146	18-8 Stainless Steel Flat Head Phillips Machine Screw, 6-32 Thread, 3/8" Length, packs of 100	McMaster-Carr	1	5.13	5.13
91771A110	18-8 Stainless Steel Flat Head Phillips Machine Screw, 4-40 Thread, 1/2" Length, packs of 100	McMaster-Carr	1	4.61	4.61
91772A105	18-8 Stainless Steel Pan Head Phillips Machine Screw, 4-40 Thread, 3/16" Length, packs of 100	McMaster-Carr	1	3.92	3.92
90107A007	Type 316 Stainless Steel Flat Washer, Number 6 Screw Size, 0.156" ID, 0.312" OD, packs of 100	McMaster-Carr	1	3.39	3.39
95584A201	Type 18-8 Stainless Steel External-Tooth Lock Washer, Number 6 Screw Size, 0.141" ID, 0.320" OD, packs of 100	McMaster-Carr	1	2.34	2.34
90257A007	Type 316 Stainless Steel Hex Nut, 6-32 Thread Size, 5/16" Wide, 7/64" High, packs of 100	McMaster-Carr	1	7.10	7.10
94812A300	Nylon 6/6 Hex Nut, 6-32 Thread Size, 5/16" Wide, 1/8" High, Off-White, packs of 100	McMaster-Carr	1	5.73	5.73
7950K28	Insulated Wire Ferrule, 14 AWG, .47" Pin Length, Blue, packs of 100	McMaster-Carr	1	5.82	5.82
7950K25	Insulated Wire Ferrule, 16 AWG, .47" Pin Length, Black, packs of 100	McMaster-Carr	1	5.25	5.25
7950K74	Insulated Wire Ferrule, 18 AWG, .47" Pin Length, Red, packs of 100	McMaster-Carr	1	5.47	5.47
7950K16	Insulated Wire Ferrule, 22-20 AWG, .39" Pin Length, Gray, packs of 100	McMaster-Carr	1	5.46	5.46
7849K31	Heat-Shrink Quick-Disconnect Terminal, Standard, Insulated Barrel, Female, 22-18 AWG, Red, packs of 25	McMaster-Carr	1	11.70	11.70
9874T11	Machine Tool Wire, 18 Gauge, Green, 25 ft. Length	McMaster-Carr	1	4.00	4.00
9874T11	Machine Tool Wire, 18 Gauge, White, 25 ft. Length	McMaster-Carr	1	4.00	4.00
9874T11	Machine Tool Wire, 18 Gauge, Black, 25 ft. Length	McMaster-Carr	1	4.00	4.00
8624T3	Mil. Spec. Wire, 150V AC, 22 Gauge, 50 Feet, Red	McMaster-Carr	1	11.23	11.23
8624T3	Mil. Spec. Wire, 150V AC, 22 Gauge, 50 Feet, Black	McMaster-Carr	1	11.23	11.23
8624T3	Mil. Spec. Wire, 150V AC, 22 Gauge, 25 Feet, Yellow	McMaster-Carr	1	6.18	6.18
288-1161-ND	CRIMP TOOL FOR 10-28AWG FERRULES	Digikey	1	209.25	209.25
2523A444	Chip-Clearing Tap for Through Holes, Standard, 4-40 Thread Size	McMaster-Carr	1	7.37	7.37
2523A446	Chip-Clearing Tap for Through Holes, Standard, 6-32 Thread Size	McMaster-Carr	1	6.20	6.20
8302A12	Chip-Clearing Tap for Through Holes, Standard, 3 x 0.5mm Thread Size	McMaster-Carr	1	9.36	9.36
				Total	**$1,357.82**

9. Github files

The most recent version of the software for the PHIP hyperpolarizer is available for download from https://github.com/coffeyam/PHIP_hyperpolarizer

10. References Used in Supporting Information

1. Coffey, A. M., Kovtunov, K. V., Barskiy, D. A., Koptyug, I. V., Shchepin, R. V., Waddell, K. W., He, P., Groome, K. A., Best, Q. A., Shi, F., Goodson, B. M. & Chekmenev, E. Y., High-resolution low-field MRI of ^{1}H and ^{13}C parahydrogen hyperpolarized molecular contrast agents. 55th Exptl. Nucl. Magn. Reson. Conf., Boston, MA, 2014.
2. Coffey, A. M., Kovtunov, K. V., Barskiy, D. A., Koptyug, I. V., Shchepin, R. V., Waddell, K. W., He, P., Groome, K. A., Best, Q. A., Shi, F., Goodson, B. M. & Chekmenev, E. Y. *Anal. Chem.* **2014**, *86*, 9042-9049.
3. Mispelter, J., Lupu, M. & Briguet, A. NMR Probeheads for Biophysical And Biomedical Experiments: Theoretical Principles And Practical Guidelines, 2006.
4. Waddell, K. W., Coffey, A. M. & Chekmenev, E. Y. *J. Am. Chem. Soc.* **2011**, *133*, 97-101.
5. Nikolaou, P., Coffey, A. M., Walkup, L. L., Gust, B. M., Whiting, N., Newton, H., Barcus, S., Muradyan, I., Dabaghyan, M., Moroz, G. D., Rosen, M. S., Patz, S., Barlow, M. J., Chekmenev, E. Y. & Goodson, B. M. *Proc. Natl. Acad. Sci. U.S.A.* **2013**, *110*, 14150-14155.
6. Goldman, M. & Johannesson, H. *C. R. Phys.* **2005**, *6*, 575-581.
7. Gridnev, I. D., Higashi, N., Asakura, K. & Imamoto, T. *J. Am. Chem. Soc.* **2000**, *122*, 7183-7194.
8. Gridnev, I. D. & Imamoto, T. *Acc. Chem. Res.* **2004**, *37*, 633-644.
9. Chekmenev, E. Y., Hovener, J., Norton, V. A., Harris, K. C., Batchelder, L. S., Bhattacharya, P., Ross, B. D. & Weitekamp, D. P. *J. Am. Chem. Soc.* **2008**, *130*, 4212-4213.
10. Shchepin, R. V., Coffey, A. M., Waddell, K. W. & Chekmenev, E. Y. *J. Am. Chem. Soc.* **2012**, *134*, 3957-3960.
11. Shchepin, R. V., Coffey, A. M., Waddell, K. W. & Chekmenev, E. Y. *Anal. Chem.* **2014**, *86*, 5601-5605.
12. Bär, S., Lange, T., Leibfritz, D., Hennig, J., Elverfeldt, D. V. & Hövener, J.-B. *J. Magn. Reson.* **2012**, *225*, 25-35.